Facilitating hydrogen atom migration via a dense phase on palladium islands to a surrounding silver surface

Christopher R. O'Connor[a], Kaining Duanmu[b,c], Dipna A. Patel[d], Eri Muramoto[e], Matthijs A. van Spronsen[a], Dario Stacchiola[f], E. Charles H. Sykes[d], Philippe Sautet[b,c], Robert J. Madix[e], and Cynthia M. Friend[a,e,1]

[a]Department of Chemistry and Chemical Biology, Harvard University, Cambridge, MA 02138; [b]Department of Chemical and Biomolecular Engineering, University of California, Los Angeles, CA 90095; [c]Department of Chemistry and Biochemistry, University of California, Los Angeles, CA 90095; [d]Department of Chemistry, Tufts University, Medford, MA 02155; [e]John A. Paulson School of Engineering and Applied Sciences, Harvard University, Cambridge, MA 02138; and [f]Center for Functional Nanomaterials, Brookhaven National Laboratory, Upton, NY 11973-5000

The migration of species across interfaces can crucially affect the performance of heterogeneous catalysts. A key concept in using bimetallic catalysts for hydrogenation is that the active metal supplies hydrogen atoms to the host metal, where selective hydrogenation can then occur. Herein, we demonstrate that, following dihydrogen dissociation on palladium islands, hydrogen atoms migrate from palladium to silver, to which they are generally less strongly bound. This migration is driven by the population of weakly bound states on the palladium at high hydrogen atom coverages which are nearly isoenergetic with binding sites on the silver. The rate of hydrogen atom migration depends on the palladium–silver interface length, with smaller palladium islands more efficiently supplying hydrogen atoms to the silver. This study demonstrates that hydrogen atoms can migrate from a more strongly binding metal to a more weakly binding surface under special conditions, such as high dihydrogen pressure.

hydrogen spillover | palladium | silver | adsorbate migration

The development of efficient and selective catalytic systems is of paramount importance in producing a broad spectrum of chemicals and fuels that are critical to the world economy. One of the major challenges in increasing the efficiency of catalysts is to achieve high selectivity while maintaining high activity. To this end, materials based on coinage metals (copper, silver, and gold) have been intensely studied because of their potential as highly selective hydrogenation catalysts (1–6). While coinage metals have potential for selective hydrogenation, they do not efficiently dissociate dihydrogen (7–9). Meanwhile, platinum group metals (nickel, palladium, platinum) facilely induce dihydrogen dissociation (7, 10); however, the selectivity for desired hydrogenation reactions is often lower on these materials (11–13). A potential solution is to combine the functionality of these two types of metals by using a bimetallic surface where hydrogen atoms can be created by the reactive metal and then supplied to the less reactive but selective metal (11–24). Specifically, palladium–silver catalysts show increased selectivity over palladium catalysts, stimulating significant discussion regarding the effect of silver on increasing selectivity (21–23, 25–30).

In order to exploit the bifunctionality of bimetallic catalyst materials, migration of chemical intermediates from the reactive component to the more selective material is necessary. Specifically, migration of hydrogen atoms formed on palladium to silver offers a way to enhance selectivity by promoting hydrogenation reactions on silver (31, 32). Hydrogen atom migration (often called "spillover") has been demonstrated across a number of metal/metal oxide and metal/metal interfaces (16–19, 33–42). However, the migration of hydrogen atoms from palladium to silver is enthalpically unfavorable, making it a difficult process. In fact, hydrogen atom migration has not been observed on

bimetallic interfaces which contain a metal component, such as gold or silver, where hydrogen atom adsorption by dihydrogen dissociation is endothermic ($\Delta H > 0$). Previous work suggested that hydrogen atom migration will not occur for alloy catalysts with single palladium atoms in gold, or silver by comparison, in the absence of adsorbates (17). At the same time, single-atom alloys of palladium in silver are selective catalysts for acrolein, nitroarene, and alkyne hydrogenation, suggesting that migration should be possible (43, 44).

Herein, we demonstrate hydrogen atom migration to a metastable site on silver following dihydrogen dissociation on a palladium island. The migration of the hydrogen atoms to silver is only observed for high hydrogen atom coverages. First, dihydrogen dissociates on palladium, forming up to ∼0.5 monolayer (ML) of hydrogen atoms on the palladium islands. Increasing the dihydrogen exposure leads to creation of a dense phase of hydrogen atoms on the palladium and the formation of metastable hydrogen atoms on silver with coverages of up to 1.05 ± 0.10 ML (palladium) and 0.56 ± 0.06 ML (silver). The palladium–silver interface length controls the rate of hydrogen atom migration to silver, where small islands of palladium are most efficient. An

Significance

The energy efficiency of catalytic processes hinges on achieving high selectivity and activity; bimetallic catalysts have potential to increase both by exploiting different chemical properties of the components. Transport of intermediates between the two metals, for example, transport of hydrogen atoms for selective hydrogenation, is required to capitalize on this bifunctionality. A mechanism for the migration of hydrogen atoms to silver from palladium is demonstrated here. Dihydrogen first dissociates on palladium, then forms a dense hydrogen phase on the palladium island. The dense phase includes weakly bound hydrogen atoms that are nearly isoenergetic with hydrogen on silver, rendering migration nearly energy neutral. The efficiency for hydrogen migration across the palladium–silver is maximized for small ensembles of palladium atoms.
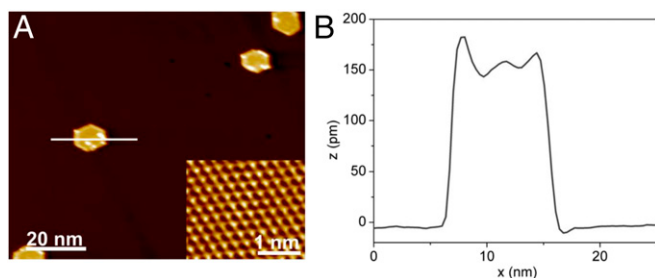
www.manaraa.com

Fig. 1. STM images at 5 K reveal that palladium islands are predominantly single layer in height when low coverages of palladium are deposited on Ag(111) at 300 K. (*A*) The STM image for 0.04 ML of palladium deposited on Ag(111) at 300 K shows hexagonal islands with an average width of 9.8 ± 1.5 nm. The width of the palladium islands is measured perpendicular to two opposite sides of the hexagon, as shown by the white line scan. *Inset* shows atomic resolution of the Ag(111) terrace. (*B*) The apparent height of a palladium island is 144.7 ± 8.2 pm based on the line scan in *A* and is consistent for all palladium coverages measured. The statistics for the STM analysis are reported in *SI Appendix*, Table S1 and Fig. S2. Imaging conditions are 0.70 V, 0.60 nA, 5 K.

energetically feasible migration pathway was discovered in which weak hydrogen atom adsorption on palladium-containing sites can facilitate migration to silver. This study clearly demonstrates that hydrogen atom migration can occur even to a metal, e.g., Ag, to which hydrogen atoms weakly bind.

Results

Imaging the Island Structure. Single-layer hexagonal islands of palladium predominantly form after palladium deposition onto Ag(111) at 300 K for total coverages below a ML, as determined by scanning tunneling microscopy (STM) experiments (Fig. 1) (45). A clean Ag(111) surface with a monoatomic step edge shows that the silver terraces are largely defect free (*SI Appendix*, Fig. S1). The apparent height of the palladium islands measures ~145 pm, which is lower than a palladium step height on Pd(111), 226 pm (46). The difference between the apparent height measured by STM and the physical height of the palladium island is due to the fact that STM images are a convolution of the physical topography of the surface and the density of electronic states of its components as well as the tip itself (47). Simply put, the palladium island is less electrically conductive than the surrounding silver host; therefore, the measured island height is lower than the actual height of a monoatomic step edge on Pd(111). The bright protrusions on the palladium islands are due to adsorption of small amounts of background gases during data acquisition at 5 K. Notably, there is very little etching of the silver surface after alloying with palladium at room temperature. As reported previously, heating to 400 K and above induces etching of silver, which migrates to cap the palladium islands (45).

Characterizing Uptake of Atomic Hydrogen by the Island-Covered Surface. There is clear evidence that dihydrogen dissociates on the palladium-covered Ag(111) surface from temperature-programmed desorption experiments (Fig. 2*A*). Distinct dihydrogen desorption features were observed at 185 and 240 K following exposure of 0.45 ML of palladium deposited on Ag(111) to dihydrogen at 150 K (Fig. 2*A*). There was no detectable adsorption of dihydrogen on clean Ag(111) under the same conditions, in agreement with previous work (48–50), demonstrating that palladium is essential for dissociation. Further, hydrogen atoms recombine and desorb in the range of 310 to 370 K from otherwise clean palladium surfaces (51), and hydrogen atoms recombine on silver in the range of 180 to 190 K (49, 50, 52). Therefore, the desorption peak at 240 K (Fig. 2*A*) is attributed to recombination of hydrogen atoms associated with the palladium islands. The lower desorption temperature for dihydrogen originating from palladium islands on Ag(111) versus Pd(111) is attributed to weaker hydrogen atom binding to the islands based on density functional theory (DFT) calculations (*SI Appendix*, Table S2). These form rapidly at low dihydrogen exposures, with their coverage increasing more slowly with increasing dihydrogen exposure (Fig. 2). The desorption feature at 185 K is attributed to hydrogen atoms associated with the silver. For convenience we define these two states of binding as $\theta_{H/Pd}$ and $\theta_{H/Ag}$, respectively.

The hydrogen atoms associated with silver begin to appear near a local hydrogen atom coverage of 0.6 ML on the palladium islands (Fig. 2*B*). For example, a 5.9 langmuir (1 langmuir = 1 L = 10^{-6} Torr s^{-1}) exposure of dihydrogen to the Ag(111) surface with 0.45 ML of palladium solely populates the sites associated with palladium (240 K). The feature at 185 K is first observed for a 59 L exposure of dihydrogen and grows in intensity with increasing exposure of dihydrogen (Fig. 2*A*). The rate of populating the 240 K feature appears to decrease significantly as the local coverage of hydrogen atoms associated with palladium, $\theta_{H/Pd}$, exceeds ~0.6 ML, as indicated by the logarithmic dependence of the coverage on the dihydrogen exposure. A similar phenomenon, reported for Pd(111), is explained by dissociation of dihydrogen by threefold adsorption site vacancy aggregates which
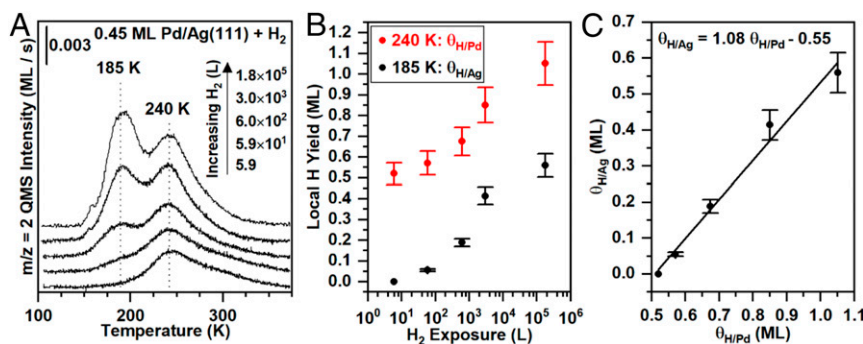

Fig. 2. Dihydrogen dissociation on palladium islands and subsequent population of a weakly bound state attributed to hydrogen atoms associated with silver depends on dihydrogen exposure. (*A*) Temperature-programmed desorption following dihydrogen exposures of 5.9, 59, 600, 3,000, and 176,000 L at 150 K. (*B*) The amounts of dihydrogen desorbing in the 240 K peak (red) and in the 185 K peak (black) increase with dihydrogen exposure up to maximum hydrogen atom coverages of 1.08 ML (240 K peak) and 0.55 ML (185 K peak). (*C*) The ratio of hydrogen atoms on the 185 K peak (silver) to those on the 240 K peak (palladium) remains constant at 1.0:1.0, starting at $\theta_{H/Pd}$ equal to 0.55 ML. Local hydrogen atom coverages (i.e., atoms of hydrogen per atoms of palladium in the islands and atoms of hydrogen per atoms of open silver) are reported as $\theta_{H/Pd}$ and $\theta_{H/Ag}$, respectively. In all experiments, 0.45 ML of palladium was deposited on Ag(111) at 300 K.

O'Connor et al.

www.manaraa.com

become vanishingly small near 0.67 ML of adsorbed hydrogen atoms (53). Accordingly, a low sample temperature that limits hydrogen atom diffusion requires a rather large dihydrogen exposure to achieve a hydrogen atom coverage of ~1 ML for both palladium islands on Ag(111) (Fig. 2) and Pd(111) (53, 54). We attribute the higher binding energy state to adsorption of hydrogen atoms on the palladium islands. The population of hydrogen atoms associated with silver, $\theta_{H/Ag}$, only begins after the local coverage of hydrogen atoms on the palladium islands reaches ~0.6 ML.

The number of hydrogen atoms adsorbed on silver vs. that on palladium ($\theta_{H/Ag}$ vs. $\theta_{H/Pd}$) follows a constant stoichiometry of 1.0:1.0 starting at $\theta_{H/Pd}$ near 0.6 ML (Fig. 2B). In our experimental conditions $\theta_{H/Pd}$ approaches a limiting value of 1.1 ML, and $\theta_{H/Ag}$ approaches 0.6 ML at the highest dihydrogen exposures (Fig. 2B). These values are in excellent agreement with published values of saturation coverages of atomic hydrogen on Pd(111) (1.0 ML) (53) and Ag(111) (0.6 ML) (49), implying that $\theta_{H/Pd}$ and $\theta_{H/Ag}$ are near saturation at these high exposures to dihydrogen.

The coverages of hydrogen atoms in the two binding states depend on the coverage of palladium (Fig. 3A). At all palladium coverages studied the palladium mainly aggregates into monolayer islands, leading to a proportional decrease in exposed silver as the palladium islands grow. Above 0.10 ML palladium bilayer high islands emerge; however, the second layer accumulation is a minority feature which does not contribute significantly to the overall growth process. The absolute coverage of the peak at 240 K increases roughly linearly with palladium coverage, providing further evidence that this peak is associated with hydrogen atom recombination on the palladium islands (Fig. 3B). The absolute coverage of hydrogen atoms in the peak at 185 K, attributed to hydrogen atoms associated with silver, increases with increasing palladium coverage, albeit more gradually than dihydrogen desorption at 240 K from palladium (Fig. 3B). The changing ratio of $\theta_{H/Pd}$ and $\theta_{H/Ag}$ over the range of palladium coverage suggests that small islands of palladium more efficiently facilitate hydrogen atom migration to silver (Fig. 3C).

The amount of hydrogen transferred from the palladium islands to the silver can be rationalized from a simple model that relates the palladium–silver interface length to the palladium coverage (*SI Appendix*, Table S1 and Fig. S2). Briefly, the steady-state concentration of hydrogen atoms on palladium and abundant open adsorption sites for hydrogen atoms on silver are assumed. The palladium–silver interface length was estimated for a given palladium coverage by establishing a relationship between palladium

coverage and hexagonal palladium island size (*SI Appendix*, Table S1 and Fig. S2). The change in palladium–silver interface length with palladium coverage agrees well with the number of hydrogen atoms on the silver surface, implying a direct relationship of the perimeter in controlling the migration of hydrogen atoms to silver (Fig. 3C). Furthermore, there is an insufficient number of interface sites to account for the amount of dihydrogen that desorbs at 185 K for large exposures of dihydrogen. Therefore, the 185 K peak is not due solely to desorption of hydrogen atoms bound to palladium edge sites, providing support for the assertion that this peak also contains hydrogen atoms bound to silver.

Clarifying the Bonding of Atomic Hydrogen to the Surface by Vibrational Spectroscopy. Further evidence for hydrogen atoms bound to palladium was obtained with high-resolution electron energy loss vibrational spectroscopy (HREELS). Prior studies show vibrational modes at both 700 and 1,080 cm^{-1} for hydrogen atoms on Pd(111) and PdAu(111) surfaces (55, 56). These modes have been assigned to the vertical and horizontal displacement of hydrogen atoms bound in threefold hollow sites on Pd(111), respectively. Similar modes were observed here for hydrogen atoms adsorbed on a multilayer (4 ML) palladium film grown on the Ag(111) surface (Fig. 4A), as would be expected for the thick, uniform Pd(111) layer. The assignments of these modes are also in agreement with DFT computations for a slab model using the palladium lattice constant, described in *Density Functional Analysis of the Bonding of Atomic Hydrogen and Its Migration on the Surface*, that yield values of 1,050 and 700 cm^{-1}.

The characteristic vibrational peaks at 1,080 and 700 cm^{-1} for hydrogen atoms bound to palladium are also observed for the silver surface covered by palladium islands ($\theta_{Pd} = 0.50$ ML) (Fig. 4B). The vibrational frequency of hydrogen atoms bound to palladium does not shift significantly for palladium islands on Ag(111) compared to Pd(111) based on DFT calculations (*SI Appendix*, Table S2). As the exposure of dihydrogen was increased from 5 to 50 L, the peak at 1,080 cm^{-1} assigned to hydrogen atoms adsorbed at threefold palladium sites increases significantly in intensity. The areas of the corresponding desorption peaks do not change proportionally over this range of dihydrogen exposures (Fig. 2), suggesting that the intensities of the vibrational peaks do not scale linearly with coverage. A similar phenomenon was observed for hydrogen atoms on Pd(311) (57).

A distinct new mode appears at the higher (50 L) dihydrogen exposure (Fig. 4B). It is notable that this feature appears at the
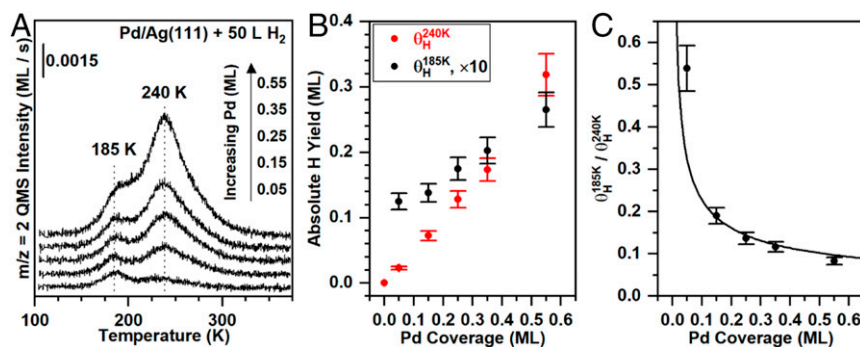

Fig. 3. The palladium coverage affects the yields of hydrogen atoms which desorb in the two different peaks at a fixed dihydrogen exposure, providing additional evidence that the 240 K peak is due to recombination from palladium islands and the 185 K peak is associated with exposed silver. (A) Temperature-programmed desorption of dihydrogen as a function of palladium coverage on Ag(111) ($\theta_{Pd} = 0.05$ to 0.55 ML) for a fixed dihydrogen exposure of 50 L. For reference, at a palladium coverage of 0.45 ML and a dihydrogen exposure of 50 L, $\theta_{H/Pd}$ is ~50% of the highest coverage achieved (Fig. 2B). (B) The absolute yields of dihydrogen in the 240 K peak (red) and the 185 K peak (black) increase nearly linearly, albeit with different slopes. The absolute yield of hydrogen atoms on silver is scaled by a factor of 10. (C) The ratio of coverages of the hydrogen atoms from the 185 K peak to those from the 240 K peak indicates that the 185 K peak is more readily populated for low palladium coverages. The solid curve illustrates the relationship between the palladium coverage and the palladium–silver interface length, assuming hexagonal palladium islands of uniform size (*SI Appendix*).
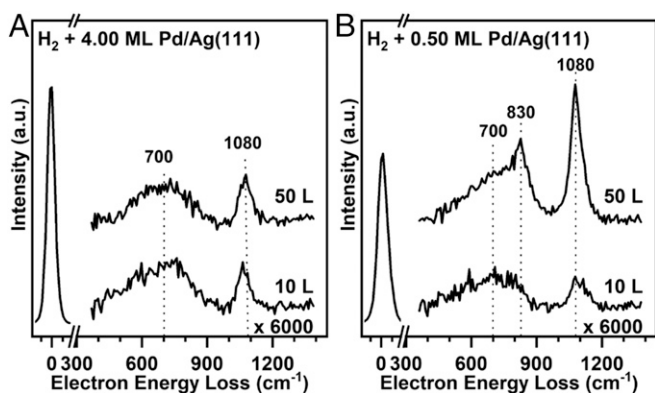
Fig. 4. Vibrational (high-resolution electron energy loss) spectra provide evidence of dihydrogen dissociation on palladium islands and migration of hydrogen atoms to silver. (*A*) Spectra taken after exposing dihydrogen to 4.00 ML of palladium on Ag(111) at 150 K are characteristic of palladium, showing peaks at 1,080 and 700 cm^{-1}, corresponding to vibrations of hydrogen atoms perpendicular and parallel to the surface, respectively. (*B*) Analogous data for palladium islands (θ_{Pd} = 0.5 ML) on Ag(111) show spectra at dihydrogen exposure of 10 and 50 L; at the higher exposure a new peak at 830 cm^{-1} is observed and is assigned to hydrogen atoms bound to silver based on comparison to literature data for hydrogen atoms on Ag(111) at 850 cm^{-1} and theoretical calculations. A quantitative interpretation of the intensities is not possible because such changes may be due to a change in sample reflectivity upon hydrogen atom adsorption and/or to the possible presence of subsurface hydrogen atoms (57). All vibrational spectra were collected at 100 K with a typical full width at half maximum of 48 cm^{-1} for the elastic peak.

dihydrogen exposure that corresponds to the emergence of the dihydrogen desorption feature at 185 K assigned to the population of the Ag(111) surface by hydrogen atoms. The vibrational mode at 830 cm^{-1} is therefore assigned to the perpendicular vibration of hydrogen atoms adsorbed on silver, in agreement with previous studies of hydrogen atoms on Ag(111) and Ag(110) and suggested by our DFT calculations on Ag(111) (801 cm^{-1}) (48, 58). These data clearly demonstrate that a new state, attributed to hydrogen atoms bound to silver, is populated at relatively high dihydrogen exposures.

Visualization of Hydrogen Atoms on Silver by Scanning Tunneling Microscopy. Direct visualization of hydrogen atoms on the Ag(111) regions amid the Pd(111) islands was achieved by scanning tunneling microscopy at 5 K, providing further evidence for hydrogen atom migration from palladium to the Ag(111) (Fig. 5). A clean

Ag(111) surface with a monoatomic step edge shows largely defect free silver terraces (*SI Appendix*, Fig. S1). After deposition of 0.05 ML of palladium on Ag(111), palladium appears as one atomic layer high hexagonal islands (Fig. 1). Following exposure to 20 L of dihydrogen, mobile depressions were observed on Ag(111), consistent with previous reports of hydrogen atom migration on CoCu(111) (40) and Cu(111) (59) (Fig. 5). Hydrogen atoms appear in STM images as depressions ($\sim$30 pm) because of the lower electron tunneling probability through the hydrogen atom–metal complexes compared to the bare metals (Fig. 5) (40, 59). The depressions on silver which are attributed to hydrogen atoms ($\sim$30 pm) are distinct from impurities observed on Ag(111) ($\sim$50 pm) (*SI Appendix*, Fig. S3). Additional evidence for the assignment of hydrogen atoms is that the $\sim$30 pm deep depressions are mobile (*SI Appendix*, Fig. S4). Under nonperturbative imaging conditions at 5 K, common impurities (e.g., S, CO, H$_2$O, etc.) are not observed to diffuse; however, hydrogen atoms can tunnel through the diffusion barrier and are mobile (59). The number of hydrogen atoms imaged on silver is small because of the low dihydrogen exposure (20 L) and the low palladium coverage (θ_{Pd} = 0.05 ML).

Density Functional Analysis of the Bonding of Atomic Hydrogen and Its Migration on the Surface. DFT calculations provide important insight into the bonding of hydrogen atoms on palladium islands as a function of coverage. The palladium overlayer was modeled by a periodic monolayer on Ag(111) in 1 × 1 epitaxy, the palladium having either the silver or the palladium lattice constant, depending on the hydrogen atom coverage. In the absence of hydrogen atom adsorbates, the palladium island has an average Pd−Pd distance close to that in bulk palladium, in line with the lower palladium chemical potential in the overlayer with the palladium lattice constant. We assume that this periodicity is maintained at low hydrogen atom coverages. Hydrogen atoms bind most strongly to threefold (face centered cubic [fcc]) sites on the palladium overlayer, with an adsorption energy of −0.84 eV (−81 KJ mol^{-1}) on the overlayer with the palladium lattice vs. −1.12 eV (−108 KJ mol^{-1}) with Pd with the silver lattice constant at a hydrogen atom coverage of 1 ML. All adsorption energies, unless otherwise noted, are for two adsorbed hydrogen atoms with respect to H$_2$ in the gas phase, having a negative value when exoenergetic. Hydrogen atom adsorption on Ag(111) is also preferred on the fcc hollow site, with an adsorption energy of +0.34 eV (+33 KJ mol^{-1}) and hence is unfavorable versus H$_2$ gas (60). The adsorption energy of hydrogen atoms is only weakly dependent on the hydrogen atom coverage on both metals. The vibrational frequencies are calculated to be 1,050 and 700 cm^{-1} for the perpendicular and parallel motions of the hydrogen atoms on a single layer of palladium on Ag(111) (with
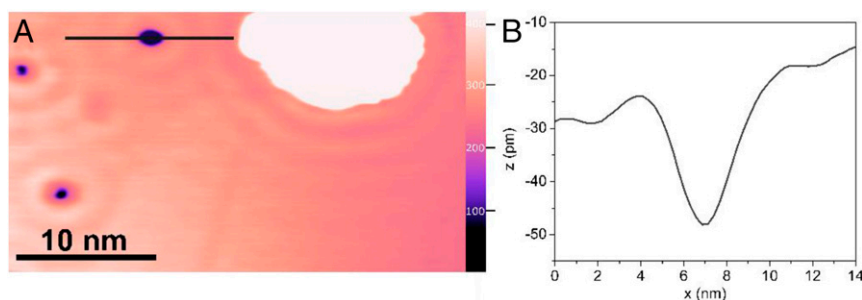

Fig. 5. Evidence for hydrogen atom migration from small palladium islands on Ag(111) is obtained from scanning tunneling microscopy experiments. (*A*) Images obtained after exposure of palladium islands (θ_{Pd} = 0.05 ML) on silver to 20 L of dihydrogen on Ag(111) at 150 K in which the palladium islands $\sim$10 nm across (white region) and hydrogen atoms present on the Ag(111) surface appear as depressions (purple) on the Ag(111) surface. (*B*) An apparent height profile along the black line scan in *A* illustrates that the features attributed to hydrogen atoms appear as depressions of $\sim$30 pm; 0.05 ML of palladium was deposited on Ag(111) at 300 K. The number of hydrogen atoms imaged on silver is small because of the low exposure of dihydrogen (20 L) and low palladium coverage (θ_{Pd} = 0.05 ML). Imaging conditions are 0.030 V, 0.020 nA, 5 K.

O'Connor et al.

www.manaraa.com

the palladium lattice constant), in excellent agreement with experiment (Fig. 4). The vibrational frequency for the mode perpendicular to the surface shifts from 1,050 cm^{-1} for the palladium lattice constant to 800 cm^{-1} if the lattice constant is expanded to the silver lattice. Hence, the predominance of the 1,080 cm^{-1} peak at low hydrogen atom coverage signifies that the palladium lattice constant is favored at such coverage.

Dihydrogen adsorption is strongly favored on palladium over silver as long as two neighboring vacant hollow sites are available. At intermediate hydrogen atom coverages, isolated unoccupied hollow sites become dominant on the palladium. When only these isolated sites are available, dihydrogen dissociation is still thermodynamically and kinetically possible if one hydrogen atom occupies a hollow site on palladium and the other hydrogen atom occupies a hollow site on silver based on DFT calculations (Fig. 6). From a thermodynamic perspective, the stabilizing adsorption energy of one hydrogen atom on this palladium site (−0.51 eV [−49 kJ mol^{-1}]) compensates the endoenergetic adsorption for the second one on silver ([+0.34 eV/2] = +0.17 eV [+16 kJ mol^{-1}]) to provide a pathway that is net energetically favorable for dissociation of the molecule (−0.34 eV [−33 kJ mol^{-1}]) when the initial surface has a hydrogen atom coverage of 0.75 ML. A pathway is calculated for such a process for the palladium overlayer with a high coverage of hydrogen atoms that leaves isolated, vacant fcc hollow sites (IS, Fig. 6). Furthermore, computations for a 12-atom palladium island on the Ag(111) (*SI Appendix*, Fig. S7) indicate that at high (1 ML) hydrogen atom coverages, the Pd−Pd distance in the island is elongated by 3.5%. Thus, because of the high coverage of hydrogen atoms at which the transfer of hydrogen atoms becomes possible to the silver, the silver lattice constant was used for the palladium overlayer to model the transfer pathway.

Additional dihydrogen molecules can dissociate on this surface (IS) by populating an available fcc site and a neighboring surface (hexagonal close packed [hcp]) site (Fig. 6, IM1), with a net favorable adsorption energy of −0.37 eV per H$_2$ (−35.7 kJ mol^{-1}), reaching a coverage of 1.25 ML. This "extra" hcp hydrogen atom (Fig. 6, IM1) is unstable with respect to 1/2 H$_2$ in the gas phase by +0.20 eV (+19.3 kJ mol^{-1}). The atom added to the hcp site is nearly equivalent in energy to a hydrogen atom bound to silver, thus establishing that migration is energetically allowed. Migration of this extra hcp hydrogen atom can occur by an exchange process, with an overall barrier of +0.31 eV (+29.9 kJ mol^{-1}), in which a neighboring fcc hydrogen atom is displaced to a hcp site (TS1, IM2), followed by refilling of that site by the extra hcp hydrogen atom taking the place of that displaced atom (TS1′, IM1′). A subsurface pathway is also energetically possible, but it is slightly less favorable (*SI Appendix*, Fig. S8). When at the edge of an island, the extra hydrogen atom can migrate to silver nearly isoenergetically (final state [FS], −0.34 eV [−32.8 KJ mol^{-1}]) (per H$_2$), as shown by calculations on Pd$_{12}$ islands (*SI Appendix*, Fig. S7). The specific modeling of the diffusion across the edge of the island model yields a relatively small activation energy (+0.33 eV [+31.8 KJ mol^{-1}]) (*SI Appendix*, Fig. S7) that is comparable to the barrier for migration.

The DFT calculations hence demonstrate that hydrogen atom migration from the palladium island to the silver surface is energetically possible as long as there is a high enough hydrogen atom coverage on the palladium island; otherwise, the adsorbed hydrogen atom is too stable and unable to migrate to silver. This result is well in line with the experimental observation of a threshold hydrogen atom coverage on palladium (0.55 ML), below which migration to silver is not seen. Theory shows that isolated vacant fcc sites are required. Since hydrogen atoms on silver are not stable versus 1/2 H$_2$ in the gas phase, formation of hydrogen atoms on silver is only possible from dihydrogen dissociation if palladium sites are simultaneously populated to render dihydrogen chemisorption an overall stabilizing effect.

The model shows that an energetically favorable process occurs when one hydrogen atom populates an fcc site on the palladium island every time that a hydrogen atom migrates to silver (Fig. 6). This is in good agreement with the experimental slope of ~1 for the ratio of desorption from the peaks attributed to palladium (240 K) and silver (185 K) (Fig. 2*C*).

Discussion

Understanding the migration of hydrogen atoms on bimetallic surfaces is crucial in promoting synergistic effects between the metal components for hydrogenation reactions. Here, models for palladium−silver catalysts established that palladium can serve as a hydrogen atom source for silver but only under specific conditions—where the hydrogen atom coverage is high on palladium and where palladium islands (not just single atoms) are present. The accessibility of weakly bound hydrogen atoms on silver could have significant implications for the design of palladium−silver catalysts for controlling the selectivity and activity of hydrogenation reactions, where silver has a high selectivity and low activity while palladium has a low selectivity but high activity. Palladium catalysts can be very selective at low conversions (61); however, palladium−silver catalysts exhibit higher selectivity than palladium catalysts at the same conversions (30). At the temperature of the catalytic reaction (e.g., room temperature), hydrogen atoms on silver will quickly recombine and desorb as dihydrogen, but a low hydrogen atom coverage on silver could exist as metastable reactive hydrogen atoms. An investigation into the reactivity of migrated hydrogen atoms on silver for hydrogenation chemistry as
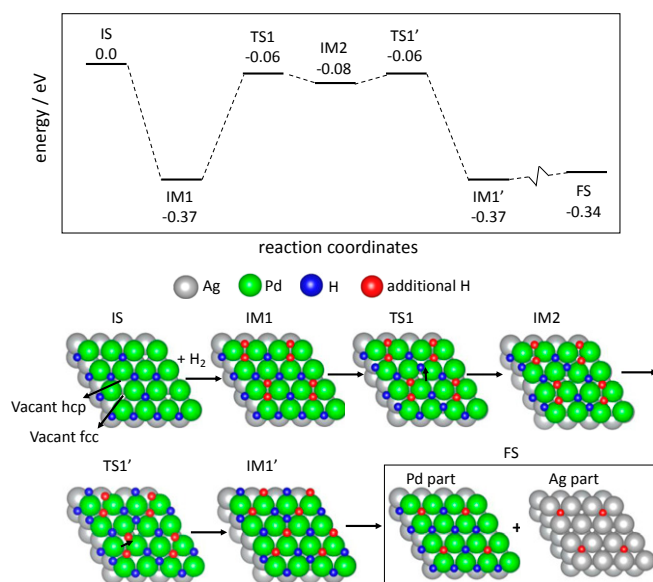

Fig. 6. An illustrative pathway for dihydrogen dissociation and hydrogen atom migration on a palladium overlayer on Ag(111) at high hydrogen atom coverage. The models corresponding to the different states depicted are below the energy diagram (silver atoms, silver; palladium atoms, green; initially adsorbed hydrogen atoms on the surface, blue; additional hydrogens from dihydrogen, red). The surface was initially covered by 0.75 ML of hydrogen atoms (blue; IS); after further dihydrogen adsorption, additional hydrogen atoms (red) occupy a fcc site and an hcp site (IM1). The hydrogen atom on a hcp site moves on the surface via a bridge site (TS1) and eventually migrates to the Ag(111) surface in the FS. The silver lattice is included in all calculations; however, it is adsorbate-free except in the FS. Since the hydrogen atom coverage is high, the silver lattice periodicity was used for the palladium overlayer (see *Density Functional Analysis of the Bonding of Atomic Hydrogen and Its Migration on the Surface*). The structure considered has a coverage of 0.75 ML on a 2 × 2 unit cell, but isolated fcc sites occur starting at 2/3 ML. All energies are given per two hydrogen atoms adsorbed, referred to as H$_2$ in the gas phase.

O'Connor et al.

a function of dihydrogen pressure and temperature is required to evaluate the possible contribution of this mechanism to a catalytic system.

Although formation of two hydrogen atoms on silver is endothermic relative to gas phase dihydrogen, previous experiments have established that hydrogen atoms remain kinetically trapped on silver when they are directly impinged on the surface at low temperature (49, 50, 52). Hence, if palladium serves as a source of hydrogen atoms, they can remain on silver, which is consistent with population of the desorption peak at 185 K (Fig. 2). The supply of hydrogen atoms to silver, though, requires high hydrogen atom coverages on the palladium islands.

The dissociation of dihydrogen and ensuing migration of hydrogen atoms to silver on the model palladium–silver system are a very complex phenomenon. At first the fcc sites of palladium are populated by hydrogen atoms. The dissociation of dihydrogen on palladium and filling of hydrogen atoms on palladium is clearly established by the 240 K peak in temperature-programmed desorption and the 1,080 cm^{-1} peak in vibrational spectroscopy. The initial population of hydrogen atoms on fcc palladium sites with a vibrational frequency of 1,080 cm^{-1} agrees with the energetics for populating fcc sites on palladium. These fcc sites will be filled until a hydrogen atom coverage of ~0.67 ML is reached, where there are limited sites for dihydrogen dissociation to create two hydrogen atoms on different fcc sites.

At high hydrogen atom coverages on palladium, population of less energetically favorable sites is possible, which enables the migration of hydrogen atoms to the nearby silver. Large dihydrogen exposures can facilitate the population of silver with hydrogen atoms, as demonstrated by direct visualization by scanning tunneling microscopy, by the 185 K peak in temperature-programmed desorption, and by the 830 cm^{-1} peaks in vibrational spectroscopy. The comparatively lower exposures of dihydrogen for the STM and vibrational spectroscopy involve a limited population of hydrogen atoms on silver, while the high exposures of dihydrogen used for the desorption experiments can achieve the saturation of hydrogen atoms on silver (~0.6 ML).

Theoretical calculations demonstrate that if a high coverage of hydrogen atoms on palladium is achieved, then the filling of weakly bound sites on palladium (hcp site, subsurface site, palladium–silver step site) is accessible, providing a pathway for hydrogen atom migration to silver. At high coverages (θ_H = 0.67 ML), dihydrogen dissociation occurs such that one hydrogen atom occupies an fcc site and the other occupies an hcp site. The hcp, subsurface, and palladium–silver step sites are all essentially isoenergetic, with the small barrier for diffusion allowing hydrogen atoms to readily explore the different surface sites. Entropic effects will further facilitate migration of hydrogen atoms from the dense phase on palladium to the dilute and mobile phase on silver. The accessibility of these more weakly bound sites agrees with the desorption of dihydrogen at 240 K from palladium, which has energetics similar to hydrogen atom adsorption on palladium–silver step sites. Further, the population of these weakly bound sites, such as subsurface sites, is dependent on sample temperature during dihydrogen exposures for Pd(111) (51); therefore, a more detailed investigation of the effect of temperature on the adsorption of dihydrogen for palladium islands on Ag(111) is warranted.

While the synergy between palladium and silver for reactions requiring hydrogen atoms has been demonstrated here for the model system consisting of palladium islands on Ag(111), there are practical challenges to implementation in a catalytic framework. First, palladium islands are required to achieve this effect. Second, the hydrogen atom coverage on palladium must be large. These two requirements necessitate reaction conditions at high pressure and relatively low temperature.

Ensuring that even small palladium islands remain on the surface requires that both synthesis and the catalyst function must occur at moderate temperatures. Heating palladium islands on Ag(111) to temperatures of 400 K, for example, may lead to capping of the palladium by silver because of the lower surface free energy of silver (45). The efficiency of supplying hydrogen atom spillover to silver is highest for the small palladium islands, suggesting that ultrasmall islands analogous to those investigated in the DFT model would be most effective (*SI Appendix*, Fig. S7). In the extreme, single atoms of palladium cannot have a vacant site for dissociation while also having the high hydrogen atom coverage necessary for spillover, indicating that there may be a minimum ensemble of palladium required.

The other important factor in exploiting the ability to supply hydrogen atoms to silver from palladium is maintaining a high coverage of hydrogen atoms on the palladium. The migration of hydrogen atoms from palladium to silver is facilitated by dihydrogen dissociation and population of weakly bound hydrogen atoms on the palladium islands. Because these states are weakly bound, high pressures of dihydrogen are required to populate them even at room temperature.

Overall, the observation of kinetically limited hydrogen atom migration facilitated by small domains of a dopant, palladium, to a material where dihydrogen dissociation is endothermic, silver, has strong implications for the design of bimetallic catalysts for reactions requiring hydrogen atoms in which selectivity is important for reactions. The accessibility of hydrogen atoms on the host metal could enable the bimetallic material to have a reaction performance like that of hydrogen atoms on the pure host metal. Such bimetallic materials for selective hydrogenation could also function to limit the overall supply of hydrogen atoms on the surface to avoid complete hydrogenation. The direct implications for controlling selectivity and activity in surface reactions are unclear—and necessitate future investigations.

In conclusion, the ability of palladium islands to facilitate hydrogen atom migration to silver when palladium islands are present was demonstrated using a comprehensive set of experimental and theoretical tools. The migration occurs because of the ability to populate weakly bound hydrogen atom adsorption states on palladium after initial dissociation of dihydrogen on palladium. The weakly bound states on palladium are nearly isoenergetic with hydrogen atoms bound to silver, rendering migration feasible. The migration occurs across the palladium–silver boundary, and accordingly, the interface length directly affects the supply of hydrogen atoms to silver, suggesting that ultrasmall palladium islands would be most effective in supplying hydrogen atoms to silver. This study clearly demonstrates that hydrogen atom migration across a bimetallic interface can provide a substantial hydrogen atom concentration on both metal components with broad implications for heterogeneous catalysis.

Materials and Methods

Experiment. Vibrational spectroscopy and temperature-programmed desorption (TPD) experiments were performed in an ultrahigh vacuum (UHV) chamber with a base pressure below 4×10^{-10} Torr. The Ag(111) single crystal (SPL) was cleaned by repeated cycles of Ar$^+$ sputtering (2.0 keV, 4 μA) and annealing (800 K). Surface cleanliness was verified using low-energy electron spectroscopy (Perkin-Elmer Phi Model 15-120 LEED Optics) and Auger electron spectroscopy (AES; Perkin-Elmer Phi 15-155 Cylindrical Auger Electron Optics). Palladium was evaporated from a palladium rod on the Ag(111) sample at 300 K using an Omicron Focus EFM 3 UHV evaporator with a constant flux of 0.15 ML min^{-1}. The coverage of palladium on Ag(111) was determined using AES. The purity of dihydrogen was confirmed by a triple-filter Hiden quadrupole mass spectrometer (Hiden HAL/3F) and by HREELS (*SI Appendix*, Fig. S9).

For dihydrogen exposures to palladium on Ag(111) a background dose at 150 K was used for HREELS experiments, and a directed dose at 150 K was used for TPD experiments. The sample was cooled to 100 K for the HREELS and TPD measurements immediately following the dihydrogen exposure. Correction for direct dosing enhancement was determined by appropriate calibrations (*SI Appendix*). All TPD experiments were performed using a constant heating rate of 3 K s^{-1}. The deconvolution of the TPD peaks at 185 and 240 K was performed using Voigt functions (*SI Appendix*). Hydrogen

O'Connor et al.

atom coverages determined in TPD experiments were quantified with mass spectrometry (62) by reference to the desorption yield of dioxygen from a saturated p(4 × 4)O-Ag(111) surface oxide (*SI Appendix*) (63). An error margin for the reported hydrogen atom coverages of ~10% is expected due to the deconvolution and quantification procedure.

HREELS experiments were performed using an LK-2000 spectrometer using a primary energy of 4.5 eV at 60° specular geometry with a specular full width at half maximum of ~6.0 meV (~48 cm^{-1}). The spectra were normalized with respect to the background counts, which has been shown to be proportional to the flux of the electron beam (64). The data were further processed by fitting and subtracting the specular peak for each spectrum to remove contributions of the specular peak from the adsorbate features. All HREELS spectra were recorded at 100 K.

STM was were performed using a low-temperature scanning tunneling microscope (Omicron Nanotechnology) under UHV with a base pressure below 1×10^{-11} Torr. A Ag(111) single crystal (Princeton Scientific) was cleaned via repeated Ar$^+$ sputtering (1.5 keV, 2μA) and annealing (1,000 K) cycles. Palladium was evaporated at room temperature using an Omicron Focus EFM 3 UHV evaporator with a constant flux of 0.1 ML min^{-1}. The Ag(111) surface prepared prior to palladium deposition consisted of Ag(111) terraces that were largely defect free separated by monatomic step edges (*SI Appendix*, Fig. S1). Dihydrogen background exposures were performed at 150 K. Scanning tunneling microscopy images at 5 K were acquired by cryogenically cooling the scanning tunneling microscope stage with liquid helium (Middlesex Gases). Notably, there is little or no alloy formation in our experiments because heating to temperatures greater than 400 K is necessary to induce alloying of the palladium and silver (45).

Theory. The hydrogen atom vibrational frequency calculations and hydrogen migration reaction on a palladium overlayer on silver were modeled by using a 2 × 2 unit cell with six layers. The bottom three layers were fixed, and the top three layers were fully optimized with a convergence threshold of 0.01 eV/Å. The palladium island model was generated by placing a 12-atom palladium island on a 5 × 5 Ag(111) surface slab with three layers. The bottom two layers were fixed, while the other atoms were fully relaxed. The Perdew–Burke–Ernzerhof functional (65) and 400 eV cutoff energy were used; the k points are 7 × 7 × 1 for the 2 × 2 unit cell model and 3 × 3 × 1 for the palladium island model. All calculations were performed with VASP (66–68).

Data Availability. All data needed to evaluate the conclusions in the paper are present in the paper, *SI Appendix*, and/or a data repository available in the Harvard Dataverse at https://doi.org/10.7910/DVN/GLEA5F. For access to materials, email the corresponding author.

1. K. Brandt, M. E. Chiu, D. J. Watson, M. S. Tikhov, R. M. Lambert, Chemoselective catalytic hydrogenation of acrolein on Ag(111): Effect of molecular orientation on reaction selectivity. *J. Am. Chem. Soc.* **131**, 17286–17290 (2009).
2. M. Bron et al., Silver as acrolein hydrogenation catalyst: Intricate effects of catalyst nature and reactant partial pressures. *Phys. Chem. Chem. Phys.* **9**, 3559–3569 (2007).
3. K. Brandt, M. E. Chiu, D. J. Watson, M. S. Tikhov, R. M. Lambert, Adsorption geometry determines catalytic selectivity in highly chemoselective hydrogenation of crotonaldehyde on Ag(111). *J. Phys. Chem. C* **116**, 4605–4611 (2012).
4. M. Pan, Z. D. Pozun, A. J. Brush, G. Henkelman, C. B. Mullins, Low-temperature chemoselective gold-surface-mediated hydrogenation of acetone and propionaldehyde. *ChemCatChem* **4**, 1241–1244 (2012).
5. M. Pan, D. W. Flaherty, C. B. Mullins, Low-temperature hydrogenation of acetaldehyde to ethanol on H-precovered Au(111). *J. Phys. Chem. Lett.* **2**, 1363–1367 (2011).
6. W. Liu et al., Catalysis beyond frontier molecular orbitals: Selectivity in partial hydrogenation of multi-unsaturated hydrocarbons on metal catalysts. *Sci. Adv.* **3**, e1700939 (2017).
7. P. J. Robinson, K. A. Holbrook, Why gold is the noblest of all the metals. *Nature* **376**, 238–240 (1995).
8. B. E. Hayden, C. L. A. Lamont, Coupled translational-vibrational activation in dissociative hydrogen adsorption on Cu(110). *Phys. Rev. Lett.* **63**, 1823–1825 (1989).
9. J. Harris, S. Andersson, C. Holmberg, P. Nordlander, The interaction of H$_2$ with metal surfaces. *Phys. Scr. T* **13**, 155–160 (1986).
10. A. T. Pasteur, S. J. Dixon-Warren, Q. Ge, D. A. King, Dynamics of hydrogen dissociation on Pt{100}: Steering, screening and thermal roughening effects. *J. Chem. Phys.* **106**, 8896–8904 (1997).
11. G. C. Bond, D. A. Dowden, N. Mackenzie, The selective hydrogenation of acetylene. *Trans. Faraday Soc.* **54**, 1537–1546 (1958).
12. E. A. Sales et al., Alumina-supported Pd, Ag and Pd-Ag catalysts: Preparation through the polyol process, characterization and reactivity in hexa-1,5-diene hydrogenation. *Appl. Catal. A Gen.* **172**, 273–283 (1998).
13. B. Yang, R. Burch, C. Hardacre, G. Headdock, P. Hu, Origin of the increase of activity and selectivity of nickel doped by Au, Ag, and Cu for acetylene hydrogenation. *ACS Catal.* **2**, 1027–1032 (2012).
14. G.-M. Schwab, *Catalysis by Metals* (Elsevier, 1963).
15. J. H. Sinfelt, Catalysis by alloys and bimetallic clusters. *Acc. Chem. Res.* **10**, 15–20 (1977).
16. M. B. Boucher et al., Single atom alloy surface analogs in Pd$_{0.18}$Cu$_{15}$ nanoparticles for selective hydrogenation reactions. *Phys. Chem. Chem. Phys.* **15**, 12187–12196 (2013).
17. F. R. Lucci et al., Controlling hydrogen activation, spillover, and desorption with Pd-Au single-atom alloys. *J. Phys. Chem. Lett.* **7**, 480–485 (2016).
18. F. R. Lucci, M. D. Marcinkowski, T. J. Lawton, E. C. H. Sykes, H$_2$ activation and spillover on catalytically relevant Pt-Cu single atom alloys. *J. Phys. Chem. C* **119**, 24351–24357 (2015).
19. H. L. Tierney, A. E. Baber, J. R. Kitchin, E. C. H. Sykes, Hydrogen dissociation and spillover on individual isolated palladium atoms. *Phys. Rev. Lett.* **103**, 246102 (2009).
20. J. Greeley, M. Mavrikakis, Alloy catalysts designed from first principles. *Nat. Mater.* **3**, 810–815 (2004).
21. N. A. Khan, S. Shaikhutdinov, H. J. Freund, Acetylene and ethylene hydrogenation on alumina supported Pd-Ag model catalysts. *Catal. Lett.* **108**, 159–164 (2006).
22. K. Mori, T. Sano, H. Kobayashi, H. Yamashita, Surface engineering of a supported PdAg catalyst for hydrogenation of CO$_2$ to formic acid: Elucidating the active Pd atoms in alloy nanoparticles. *J. Am. Chem. Soc.* **140**, 8902–8909 (2018).
23. F. Studt et al., On the role of surface modifications of palladium catalysts in the selective hydrogenation of acetylene. *Angew. Chem. Int. Ed. Engl.* **47**, 9299–9302 (2008).
24. G. Kyriakou et al., Isolated metal atom geometries as a strategy for selective heterogeneous hydrogenations. *Science* **335**, 1209–1212 (2012).
25. C. N. Thanh, B. Didillon, P. Sarrazin, C. Cameron, "Selective hydrogenation catalyst and a process using that catalyst." US Patent 6,054,409 (2000).
26. G. X. Pei et al., Ag alloyed Pd single-atom catalysts for efficient selective hydrogenation of acetylene to ethylene in excess ethylene. *ACS Catal.* **5**, 3717–3725 (2015).
27. R. N. Lamb et al., Surface characterisation of Pd-Ag/Al$_2$O$_3$ catalysts for acetylene hydrogenation using an improved XPS procedure. *Appl. Catal. A Gen.* **268**, 43–50 (2004).
28. M. Takht Ravanchi, S. Sahebdelfar, Pd-Ag/Al$_2$O$_3$ catalyst: Stages of deactivation in tail-end acetylene selective hydrogenation. *Appl. Catal. A Gen.* **525**, 197–203 (2016).
29. A. Pachulski, R. Schödel, P. Claus, Performance and regeneration studies of Pd-Ag/Al$_2$O$_3$ catalysts for the selective hydrogenation of acetylene. *Appl. Catal. A Gen.* **400**, 14–24 (2011).
30. Q. Zhang, J. Li, X. Liu, Q. Zhu, Synergetic effect of Pd and Ag dispersed on Al$_2$O$_3$ in the selective hydrogenation of acetylene. *Appl. Catal. A Gen.* **197**, 221–228 (2000).
31. M. T. Darby, M. Stamatakis, A. Michaelides, E. C. H. Sykes, Lonely atoms with special gifts: Breaking linear scaling relationships in heterogeneous catalysis with single-atom alloys. *J. Phys. Chem. Lett.* **9**, 5636–5646 (2018).
32. M. T. Greiner et al., Free-atom-like d states in single-atom alloy catalysts. *Nat. Chem.* **10**, 1008–1015 (2018).
33. R. Prins, Hydrogen spillover. Facts and fiction. *Chem. Rev.* **112**, 2714–2738 (2012).
34. R. B. Levy, M. Boudart, The kinetics and mechanism of spillover. *J. Catal.* **32**, 304–314 (1974).
35. J. Park et al., Investigation of the support effect in atomically dispersed Pt on WO$_{3-x}$ for utilization of Pt in the hydrogen evolution reaction. *Angew. Chem. Int. Ed. Engl.* **58**, 16038–16042 (2019).
36. W. Karim et al., Catalyst support effects on hydrogen spillover. *Nature* **541**, 68–71 (2017).
37. N. Doudin et al., Understanding heterolytic H$_2$ cleavage and water-assisted hydrogen spillover on Fe$_3$O$_4$(001)-supported single palladium atoms. *ACS Catal.* **9**, 7876–7887 (2019).
38. D. W. Goodman, J. T. Yates, C. H. F. Peden, The reaction of atomic copper with chemisorbed hydrogen on ruthenium. *Surf. Sci.* **164**, 417–424 (1985).
39. M. D. Marcinkowski et al., Controlling a spillover pathway with the molecular cork effect. *Nat. Mater.* **12**, 523–528 (2013).
40. E. A. Lewis, M. D. Marcinkowski, C. J. Murphy, M. L. Liriano, E. C. H. Sykes, Hydrogen dissociation, spillover, and desorption from Cu-supported Co nanoparticles. *J. Phys. Chem. Lett.* **5**, 3380–3385 (2014).
41. Y. Yao, D. W. Goodman, Direct evidence of hydrogen spillover from Ni to Cu on Ni-Cu bimetallic catalysts. *J. Mol. Catal. Chem.* **383–384**, 239–242 (2014).
42. C. R. O'Connor et al., Hydrogen migration at restructuring palladium-silver oxide boundaries dramatically enhances reduction rate of silver oxide. *Nat. Commun.* **11**, 1844 (2020).
43. P. Aich et al., Single-atom alloy Pd-Ag catalyst for selective hydrogenation of acrolein. *J. Phys. Chem. C* **119**, 18140–18148 (2015).
44. G. Vilé et al., A stable single-site palladium catalyst for hydrogenations. *Angew. Chem. Int. Ed. Engl.* **54**, 11265–11269 (2015).
45. M. A. van Spronsen et al., Dynamics of surface alloys: Rearrangement of Pd/Ag(111) induced by CO and O$_2$. *J. Phys. Chem. C* **123**, 8312–8323 (2019).

O'Connor et al.

46. G. Zheng, E. I. Altman, Oxidation of Pd(111). *Surf. Sci.* **462**, 151–168 (2000).
47. C. J. Chen, *Introduction to Scanning Tunneling Microscopy* (Oxford University Press, 1993).
48. D. Holmes Parker, M. E. Jones, B. E. Koel, Determination of the reaction order and activation energy for desorption kinetics using TPD spectra: Application to D$_2$ desorption from Ag(111). *Surf. Sci.* **233**, 65–73 (1990).
49. G. Lee *et al.*, Chemisorption of hydrogen on the Ag(111) surface. *J. Vac. Sci. Technol. A* **12**, 2119–2123 (1994).
50. G. Lee, E. W. Plummer, Interaction of hydrogen with the Ag(111) surface. *Phys. Rev. B Condens. Matter* **51**, 7250–7261 (1995).
51. G. E. Gdowski, T. E. Felter, R. H. Stulen, Effect of surface temperature on the sorption of hydrogen by Pd(111). *Surf. Sci.* **181**, L147–L155 (1987).
52. X. L. Zhou, J. M. White, B. E. Koel, Chemisorption of atomic hydrogen on clean and Cl-covered Ag(111). *Surf. Sci.* **218**, 201–210 (1989).
53. T. Mitsui, M. K. Rose, E. Fomin, D. F. Ogletree, M. Salmeron, Dissociative hydrogen adsorption on palladium requires aggregates of three or more vacancies. *Nature* **422**, 705–707 (2003).
54. T. Mitsui, M. K. Rose, E. Fomin, D. F. Ogletree, M. Salmeron, Hydrogen adsorption and diffusion on Pd(1 1 1). *Surf. Sci.* **540**, 5–11 (2003).
55. H. Conrad, M. E. Kordesch, R. Scala, W. Stenzel, Surface resonances on Pd(111)/H observed with HREELS. *J. Electron Spectrosc. Relat. Phenom.* **38**, 289–298 (1986).
56. N. Takehiro, P. Liu, A. Bergbreiter, J. K. Nørskov, R. J. Behm, Hydrogen adsorption on bimetallic PdAu(111) surface alloys: Minimum adsorption ensemble, ligand and ensemble effects, and ensemble confinement. *Phys. Chem. Chem. Phys.* **16**, 23930–23943 (2014).
57. D. Farías, P. Schilbe, M. Patting, K. H. Rieder, The transition of chemisorbed hydrogen into subsurface sites on Pd(311). *J. Chem. Phys.* **110**, 559–569 (1999).
58. P. T. Sprunger, E. W. Plummer, Interaction of hydrogen with the Ag(110) surface. *Phys. Rev. B Condens. Matter* **48**, 14436–14446 (1993).
59. A. D. Jewell *et al.*, Quantum tunneling enabled self-assembly of hydrogen atoms on Cu(111). *ACS Nano* **6**, 10115–10121 (2012).
60. P. Ferrin, S. Kandoi, A. U. Nilekar, M. Mavrikakis, Hydrogen adsorption, absorption and diffusion on and in transition metal surfaces: A DFT study. *Surf. Sci.* **606**, 679–689 (2012).
61. H. R. Adúriz, P. Bodnariuk, M. Dennehy, C. E. Gigola, Activity and selectivity of Pd/α-Al$_2$O$_3$ for ethyne hydrogenation in a large excess of ethene and hydrogen. *Appl. Catal.* **58**, 227–239 (1990).
62. B. Xu, R. J. Madix, C. M. Friend, Achieving optimum selectivity in oxygen assisted alcohol cross-coupling on gold. *J. Am. Chem. Soc.* **132**, 16571–16580 (2010).
63. A. Klust, R. J. Madix, Mesoscopic restructuring and mass transport of metal atoms during reduction of the Ag(111)-p(4x4)-O surface with CO. *J. Chem. Phys.* **126**, 084707 (2007).
64. C. G. Williams *et al.*, Metal-ligand complexation through redox assembly at surfaces characterized by vibrational spectroscopy. *J. Phys. Chem. C* **121**, 13183–13190 (2017).
65. J. P. Perdew, K. Burke, M. Ernzerhof, Generalized gradient approximation made simple. *Phys. Rev. Lett.* **77**, 3865–3868 (1996).
66. G. Kresse, J. Furthmüller, Efficiency of ab-initio total energy calculations for metals and semiconductors using a plane-wave basis set. *Comput. Mater. Sci.* **6**, 15–50 (1996).
67. G. Kresse, J. Hafner, Ab initio molecular dynamics for liquid metals. *Phys. Rev. B Condens. Matter* **47**, 558–561 (1993).
68. G. Kresse, J. Hafner, Ab initio molecular-dynamics simulation of the liquid-metal-amorphous-semiconductor transition in germanium. *Phys. Rev. B Condens. Matter* **49**, 14251–14269 (1994).

O'Connor et al.

www.manaraa.com